Journal of Hazardous Materials 170 (2009) 374–381

Contents lists available at ScienceDirect

Journal of Hazardous Materials

journal homepage: www.elsevier.com/locate/jhazmat

An oilwell cement slurry additivated with bisphenol diglycidil ether/isophoronediamine—Kinetic analysis and multivariate modelings at slurry/HCl interfaces

Antonio R. Cestari*, Eunice F.S. Vieira, Andréa M.G. Tavares, Marcos A.S. Andrade Jr.

Laboratory of Materials and Calorimetry, Department of Chemistry/CCET, Sergipe Federal University, Av. Marechal Rondon S/N, Jardim Rosa Elze, CEP 49100-000, São Cristóvão, Sergipe, Brazil

ARTICLE INFO

Article history:
Received 3 March 2009
Received in revised form 20 April 2009
Accepted 21 April 2009
Available online 3 May 2009

Keywords:
Cement slurries
Epoxy resins
Multivariate analysis
Environmental protection

ABSTRACT

Loss of zonal isolation in oilwell cementing operations leads to safety and environmental problems. The use of new cement slurries can help to solve this problem. In this paper, an epoxy-modified cement slurry was synthesized and characterized. The features of the modified slurries were evaluated in relation to a standard cement slurry (w/c = 0.50). A kinetic study of HCl interaction with the slurries was carried out using cubic molds. The Avrami kinetic model appears to be the most efficient in describing kinetic isotherms obtained from 25 to 55 °C. Type of slurry, HCl concentration and temperature effects were also evaluated in HCl adsorption onto cement slurries considering a 2^3 full factorial design. From the statistical analysis, it is inferred that the factor "HCl concentration" has shown a profound influence on the numerical values of the Avrami kinetic constants. However, the best statistical fits were found using binary and tertiary interactive effects. It was found that the epoxy-modified cement slurry presents a good potential to be used in environmental-friendly oilwell operations.

1. Introduction

Portland cement is used in large quantities to "grout" oilwells. The cement slurry is placed between a metal liner and the walls of the borehole to provide support for the liner and a seal to prevent the migration of gas and loss of zonal isolation along the outside of the liner [1]. If the cement slurry does not provide a good seal, loss of zonal isolation leads to safety and environmental problems [1–3]. Long-term performance of the cement slurries is of great concern. However, several oilwells have been observed, after routine acidification operations, to exhibit well zonal intercommunication problems, due to reactions between the hardened slurry in the annulus and the acidic solution. The protective characteristics of oilwell cements are in practice controlled by the addition of additives [1–4].

Epoxy resins are used to provide a good wettability of the cementitious substrate. The polymeric structure is useful to promote physico-chemical interactions and ensure an optimal level of adhesion between the mineral and organic phases of cement slurries [5,6]. At the present almost 90% of the world production of epoxy resins is based on the reaction between bisphenol A (2,2-bis(4′-hydroxyphenyl)propane and epichlorohydrin [2–4,6]. Epoxy cement mortars are composed of emulsified bisphenol A epoxy resin, cement and fine aggregates. In some cases, the epoxy cement mortars with hardeners, which are Lewis bases in nature (generally, organic acids or amines), have some properties that are better than the mortars without a hardener. The conventional epoxy cement mortars with a hardener must have polymer content higher than 40% to achieve good mechanical properties and durability. The epoxy resins can also harden in the presence of alkalis formed from the hydration of cement [1,5,6].

Experiments have shown that the corrosion resistance of cement slurries depends on the type and chemical composition of the cement as well as the pH of the attacking acid [7]. The rate of corrosion is determined by the concentration of the acid and the type of cement composition. The dissolution of ferrite or aluminate hydrates and the corresponding loss of Fe^{3+} and Al^{3+} are slow and occur at low pH [8].

Taking into account that interactions at hardened cement/acidic species interfaces are of complex nature, new approaches should be used for their characterization. Statistical methods of optimization and analysis such as factorial design and response surface analysis have been applied to different systems because of their capacities to extract relevant information from systems while requiring a minimum number of experiments. Since substantial interactions among the experimental variables are frequently evidenced, which can predominate over main factor effects, univariate optimization strategies have been shown to be relatively inadequate in these

* Corresponding author. Tel.: +55 79 21056656; fax: +55 79 21056684.
E-mail address: cestari@ufs.br (A.R. Cestari).

0304-3894/$ – see front matter © 2009 Elsevier B.V. All rights reserved.
doi:10.1016/j.jhazmat.2009.04.085

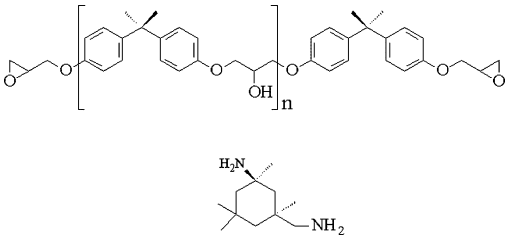

Fig. 1. Chemical structures of the epoxy resin (above) and the hardener (below).

kinds of studies at cement/solution interfaces [9]. Besides economizing experimental efforts, multivariate methods are capable of measuring interaction effects as well as the individual effect of each experimental factor on response properties of interest in the most precise way possible [9]. However, to our knowledge, despite the large number of works concerning interaction of acidic species with cemented bodies, statistical analyses of the role of experimental parameters on the interaction kinetic parameters such as temperature and solute concentration, as well as their interactions, are seldom and scattered in literature.

In this work, kinetic parameters of HCl interaction with an epoxy-modified cement slurry and a standard cement slurry were obtained and evaluated. In addition, some kinetic results were analyzed and modeled using a 2^3 full factorial design.

2. Materials and methods

2.1. Materials and reagents

Powder cement (200–325 mesh, Class A) from Cimesa (Laranjeiras-SE, Brazil) was used. The bisphenol A epoxy resin, commercially available as Araldite GY279, as well as its hardener (Aradur 2963) were supplied by The Huntsman Co. Special Resins. The chemical structures of the resins and the hardener are shown in Fig. 1. The compositions of the resin and the hardener were shown in a previous published work [10].

2.2. Preparation of the cement slurries

The mixing procedure adopted was in accordance with the American Petroleum Institute (API) practice, and consisted of mixing the cement, epoxy resin and hardener at 4000 rpm during 20 s, then mixing for 30 s at 12,000 rpm [11,12]. In order to avoid uncompleted polymerization, the proportion of epoxy resin/hardener was 1:2. The cement and water were used to obtain the standard cement slurry. The amounts of the components of the slurries were calculated in relation to a final density of the cured slurries from 1.50 to 2.00 g cm^{-3} [10–12]. The cement slurries were cast into cubic molds with 5.08 cm sides and cured in water for 30 days before use. The slurries are hereafter denominated, for simplicity, as standard slurry (cement and water) and GY279 (Araldite GY279 + Aradur 2963).

2.3. Characterization of the slurries

The thermogravimetric analyses (TG and DTG) were made using about 10 mg of material, under oxidative atmosphere from 25 to 800 °C, in a SDT 2960 thermoanalyzer, from TA Instruments. DSC analyses were performed in sealed Al pans, using about 10 mg of material, under oxidative atmosphere from 25 to 600 °C. DRX-ray analyses were performed in a Rigaku diffractometer, in the 2θ range from 5° to 80° (accumulation rate of 0.02 min^{-1}), using Cu Kα radiation.

2.4. Kinetic experiments

The interaction experiments were performed using an isothermal water bath [10], from 25 to 55 ± 0.1 °C. In a typical experiment, a cubic cemented sample was put in contact with 400 mL of 0.01 or 0.10 mol L^{-1} HCl solution in a glass beaker at a determined temperature. At predetermined times, the HCl concentrations in the solutions were determined by acid–base titrations using 0.01 mol L^{-1} NaOH solutions. All determinations were carried out in triplicate runs.

The amounts of acidic species adsorbed were calculated using the expression [8]:

$$Q_t = \frac{(C_i - C_t)V}{m} \quad (1)$$

where Q_t is the fixed quantity of acidic species per gram of slurry at a given time t in mol g^{-1}, C_i is the initial concentration of acidic species in mol L^{-1}, C_t is the concentration of acidic species at a given time t in mol L^{-1}, V is the volume of the solution in L and m is the mass of slurry in g.

The statistical calculations (t-tests, F-tests, analysis of variance (ANOVA) and multiple regressions) were performed using the software packages ORIGIN®, and the Statistica®, both release 7.0.

3. Results and discussion

3.1. Some initial considerations

The composition of oilwell cement slurries is usually based upon four principal mineral phases [1]: tricalcium silicate (Ca_3SiO_5), dicalcium silicate (Ca_2SiO_4), tricalcium aluminate ($Ca_3Al_2O_6$) and a calcium aluminoferrite of more variable composition. The calcium silicate hydrate formed, known as C–S–H, is a very poorly crystalline non-stoichiometric material consisting principally of dimeric units at first, but which subsequently slowly polymerize after a few days to give higher linear units like pentamer and thence octamer.

Tricalcium silicate is the principal cementing phase, whereas dicalcium silicate (usually in the β-form) reacts at a much slower rate to form similar hydration products. The hydration products from the tri- and β-dicalcium silicate phases at up to ∼100 °C do not differ essentially from those formed at ambient temperature. The rate of hydration of Portland cement increases with increasing temperature, especially at lower degrees of hydration, whereas this effect becomes less pronounced as the hydration progresses [1]. Only the hydration of dicalcium silicates was found to be accelerated significantly even months after mixing with water. No changes in the mechanism of hydration have been reported in the temperature range from ambient to 90 °C. At elevated temperatures the hydration of β-dicalcium silicate is accelerated in relation to that of tricalcium silicate, which could be related to the high solubility of silica and low solubility of calcium hydroxide under these conditions.

Some calcium hydroxide is present at the beginning of hydration, where the aqueous phase of the cement slurry can be considered for simplicity as essentially a limewater medium, being derived from some hydration of the small free lime content [1,5–7] as follows:

$$CaO + H_2O \rightarrow Ca(OH)_2 \quad (2)$$

The alkali metal ions from the sulfates readily enter to solution when the cement is mixed with water and accelerate the early hydration reactions, particularly those of tricalcium silicate and tricalcium aluminate.

The epoxy-amine addition is formally a bi-molecular stepwise reaction that takes place opening the oxirane rings of the epoxy component by hydrogen atoms of the amine component, as shown

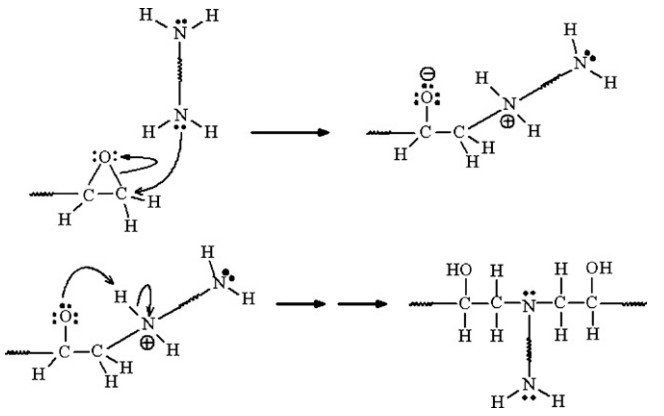

Fig. 2. Chemical mechanism proposed for the reaction of a epoxy resin and a primary amine as the hardener.

in Figs. 2 and 3 [15]. Polymer networks are formed from functional precursors by reactions between their functional groups resulting in bond formation. Branched and cross-linked structures are formed by this process. If bi- or higher functional epoxies react with tri- or higher functional amines, then rigid thermosetting polymers can be formed. The system consisting of a bi-functional epoxy and tetra-functional diamine is a typical example which has been often used for modeling purposes. The primary amine sites in this system act as chain extenders while the secondary amines produce the branches [15].

In general, as the transition temperature (*Tg*) of a resin system is raised, a decrease in toughness and dimensional stability is observed. This depends on the fact that these properties are all related to the cross-link density of the cured resins, which rigidifies the molecular network, decreases its deformability, and increases the process-induced shrinkage [16]. Aromatic and cyclic amines generally lead to thermosets with higher *Tg*s, superior thermal resistance and mechanical performances. If aliphatic acids are used as curing agents more flexible materials will obtained with lower *Tg*s.

3.2. Characterization features of the cement slurries

The TG/DTG curves of the cement slurries are presented in Figs. 4 and 5. The identification of mineral components and their quantification, using DTA/TGA is difficult and often may be impossible due to overlapping processes. The TG curve of the standard slurry presents three major mass losses steps: (a) release of the evaporable part of the adsorbed water until approximately 150 °C; (b) $Ca(OH)_2$ dehydration, between 400 and 450 °C; (c) decomposition of the carbonate phases (typically calcium carbonate) above 450 °C [1,10–12]. The slurry GY279 presents higher mass losses in relation to the standard slurry due to the organic components of these slurries. The decrease in the first mass loss step suggests that the epoxy-slurries have lower water affinity than the standard slurry due to the presence of organic hydrophobic groups of the epoxy resin [1,10–12]. The analysis of the DTG curves of the slurries also suggests significant compositional differences of the materials.

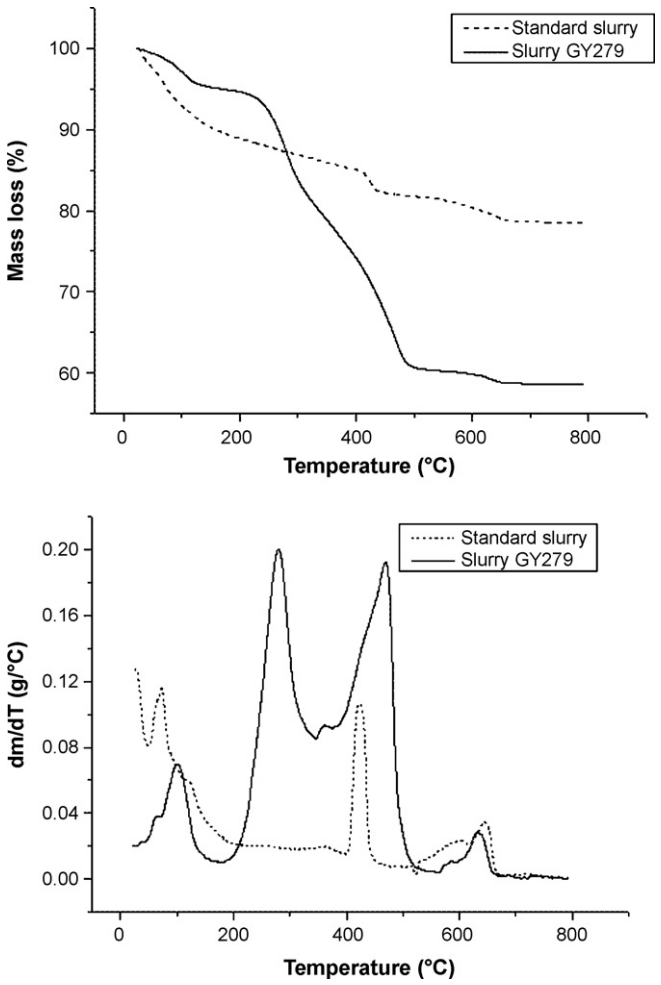

Fig. 4. TG (above) and DTG (below) curves of the standard slurry and the slurry GY279.

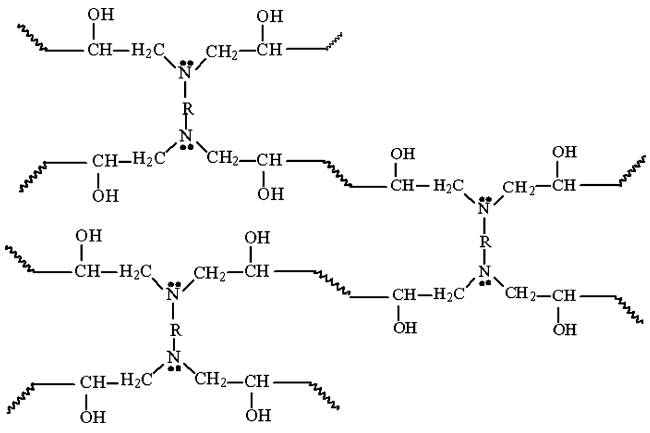

Fig. 3. Idealized structure of polymerized amine-cross-linked epoxy resins.

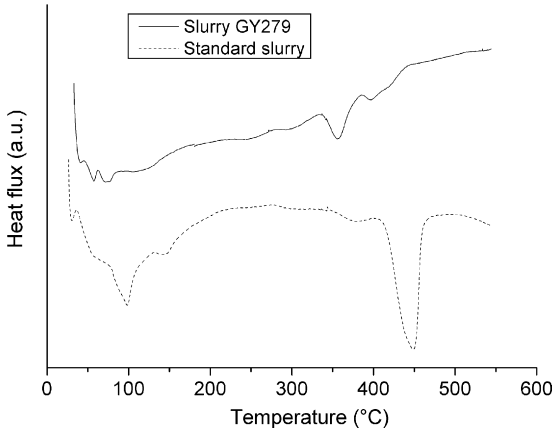

Fig. 5. DSC curves of the standard slurry and the slurry GY279.

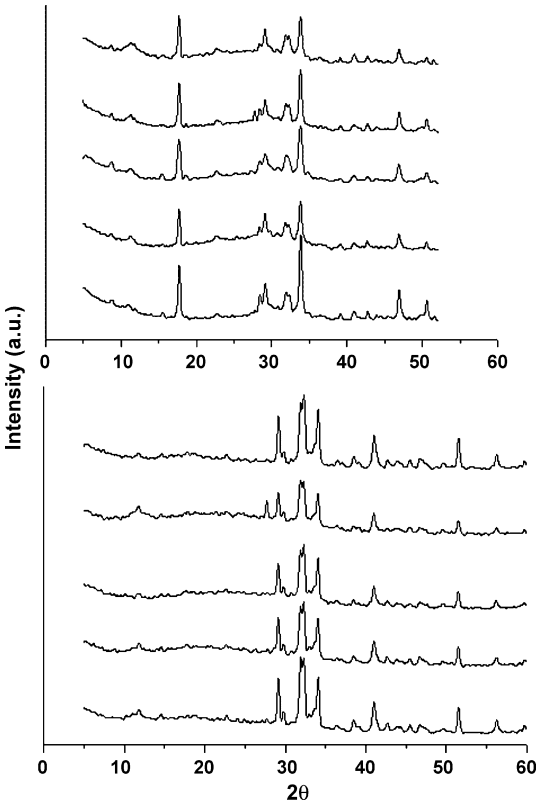

Fig. 6. DRX diffractograms of the standard slurry (above) and the slurry GY279 (below) as a function of curing time.

The DSC curves of the slurries are presented in Fig. 5. The endothermic peaks in the DSC curve of the standard slurry, located at about 50–220 °C, as well as the at 350–500 °C have been attributed to the evaporation of physically and chemically bound water in C–S–H gel phase and the portlandite dehydroxylation, respectively [10–12]. On the other hand, the slurry GY279 presents a maximum endothermic peak located at about 350 °C, due, probably, to the decomposition of the organic structure of the epoxy resin. The intimate interactions between the mineral phases of the slurries and the cross-linked epoxy adhesive also lead to an increase in the *Tg* of the polymer network (details not shown) from about 50 °C (bulk resin) to about 75 °C (cement slurry-linked resin). This phenomenon accounts for the reduced mobility of macromolecular chains of the resins in the interfacial regions with the cured slurries [15,16].

The XDR profiles of the slurries are presented in Fig. 6. In general, no changes were observed in relation to the hydration time of the slurries. Crystalline materials belonging to the crystallographic systems of higher symmetry, such as the isometric, tend to give strong patterns containing relatively few lines, while materials of lower crystal symmetry give weaker patterns and a greater number of lines. However, reflections from different minerals coincide or overlap [14].

The main products common to all slurries are portlandite, ettringite and ill crystallized C–S–H ($2\theta = 25–35°$) [10–14]. For the standard slurry, it is suggested the formation of major products of portlandite [$Ca(OH)_2$] ($2\theta = 18°$), calcite and β-tricalcium silicate (C_3SH, [$Ca_6Si_2O_7(OH)_6$]) ($2\theta = 28°$), ettringitte ($3CaO{\cdot}Al_2O_3{\cdot}3CaSO_4{\cdot}32H_2O$) ($2\theta = 34°$) and a mixture of α-dicalcium silicate (C_2SH, [$Ca_2SiO_4{\cdot}H_2O$]) and portlandite ($2\theta = 47°$) [14]. For the slurry GY279, the major products are α-C_2SH ($2\theta = 34°$) and tobermorite [$Ca_5Si_5Al(OH)O_{17}{\cdot}5H_2O$] (a strength retrogression inhibitor presents in cured oilwell slurries [1]), and mixtures of calcite and aragonite ($2\theta = 28°$, 42° and 52°). The XRD patterns have suggested absence of portlandite in slurry GY279, as observed earlier by TG/DTG and DSC analyses. In paste hydration of C_3S most of the calcium hydroxide precipitates in the form of crystals of portlandite. The absence of portlandite in slurry GY279 seems to be related to the low concentration of Ca^{2+} and OH^- ions in the liquid phase in the curing processes of the epoxy-modified cement slurries. Thus, in highly diluted suspensions containing Ca^{2+} and OH^- ions, in which the saturation level is not attained, calcium hydroxide (portlandite) is not formed in appreciable (or detectable) amounts [1]. Thus, the presence of water is a key point to form portlandite.

Some features of the microstructure of the slurries have changed after HCl attack (details not shown). For the X-ray patterns, the structures decreased their crystalline characteristics. Thus, XRD does not allow the determination of the slurries constituents. Similar results were also observed earlier [17]. For the standard slurry, portlandite peaks had disappeared, whereas the peaks of C_3S and C_2S were being increased. For slurry GY279, C–S–H halos with maximum peaks at about $2\theta = 18°$ were observed.

3.3. Kinetic of HCl interaction onto the slurries

Figs. 7 and 8 show the HCl adsorption amounts on the slurries, which are progressively occupied by the acid. As shown, the amount of HCl adsorbed increases with contact time and it remains constant after an equilibrium contact time in relation to a given initial HCl concentration and temperature. The interaction of HCl increased with increasing initial HCl concentration in solution. For the standard slurry, when the initial HCl concentration was 0.01 mol L^{-1}, it is observed from Figs. 8 and 9 that the amount of adsorbed HCl on slurries increased from 25 to 45 °C. However, for the GY279

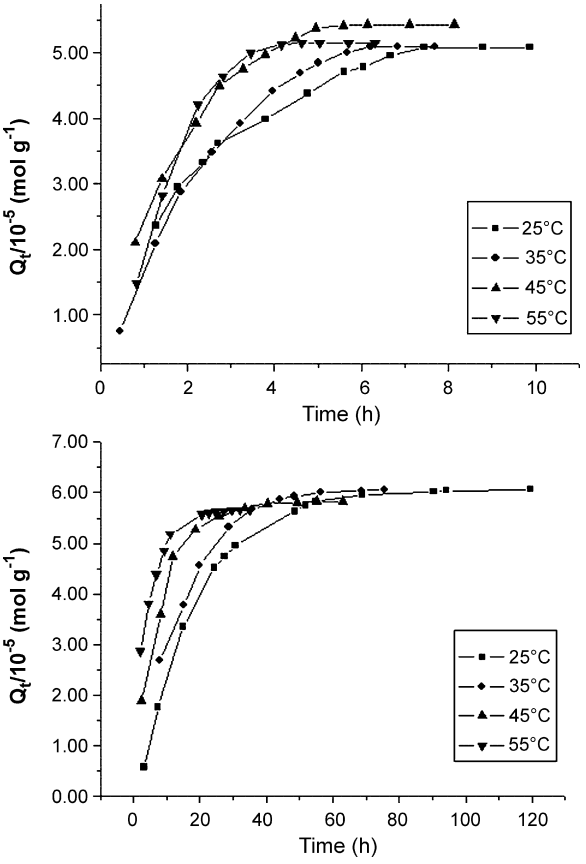

Fig. 7. Adsorption profiles of HCl on the standard slurry in relation to the contact time, at different temperatures. Initial [HCl] = 0.01 mol L^{-1}.

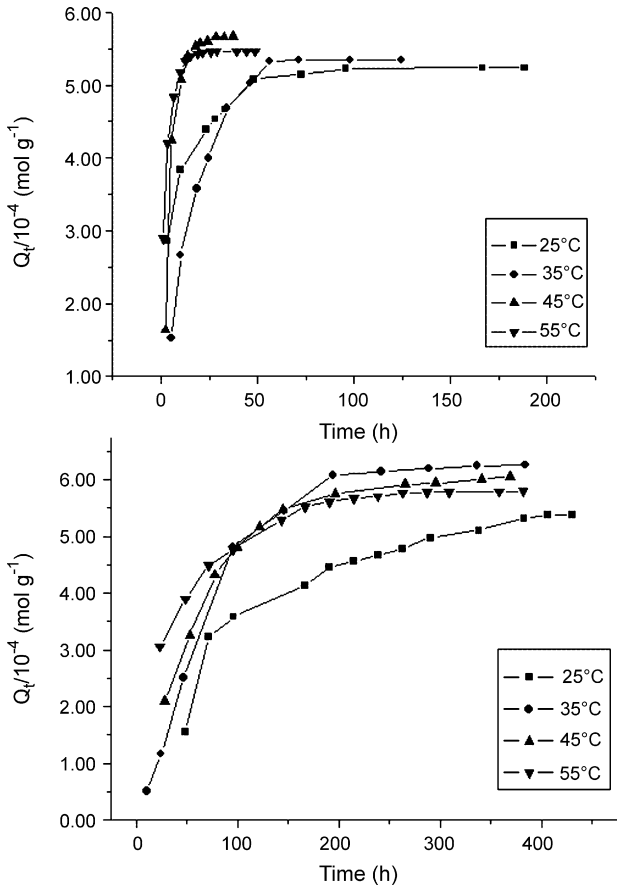

Fig. 8. Adsorption profiles of HCl on the standard slurry in relation to the contact time, at different temperatures. Initial [HCl] = 0.1 mol L^{-1}.

slurry, the effects of initial HCl concentration and temperature are more complex. For example, when the initial HCl concentration was 0.1 mol L^{-1}, the HCl interaction increased from 25 to 35 °C and decreased from 35 to 55 °C. These results seem to indicate that the HCl interaction for GY279 slurry is exothermic from 25 to 35 °C and endothermic from 35 to 55 °C.

Interaction processes at solid/solution interfaces typically take place taking into account two main aspects. Firstly, the adsorbate is transferred from the solution to the adsorbent solid surface. The last stage is related to the diffusion of the adsorbed species within the pores of material, binding the pores and capillary spaces. However, both mentioned interaction processes can present different interaction kinetic rates, which are related mainly to variations of solute concentration and adsorption temperature.

Traditionally, the interaction kinetics at solid/solution interfaces is described following the expressions originally given by Lagergren, which are special cases for the general Langmuir rate equation [18]. A simple kinetic analysis is the pseudo-first-order equation in the form:

$$\frac{dQ_t}{dt} = k_1(Q_e - Q_t) \tag{3}$$

where k_1 is the pseudo-first-order rate constant that relates to the amount of acid adsorbed by the solid phase and Q_e denotes the amount of adsorption at equilibrium. After definite integration and applying the initial conditions $Q_t = 0$ at $t = 0$ and $Q_t = Q_t$ at $t = t$, Eq. (3) becomes

$$\ln(Q_e - Q_t) = \ln(Q_e) - k_1 t \tag{4}$$

In addition, a pseudo-second-order equation based on adsorption equilibrium capacity may be expressed in the form:

$$\frac{dQ_t}{dt} = k_2(Q_e - Q_t)^2 \tag{5}$$

where k_2 is the pseudo-second-order rate constant that relates to the amount of acid adsorbed by the solid phase. Integrating Eq. (5) and applying the initial conditions, we have:

$$\frac{1}{Q_e - Q_t} = \frac{1}{Q_e} + k_2 t \tag{6}$$

or equivalently,

$$\frac{t}{Q_t} = \frac{1}{k_2 Q_e^2} + \frac{1}{Q_e} t \tag{7}$$

It should be noted that, compared to Eqs. (6) and (7) has an advantage that k_2 and Q_e can be obtained from the intercept and slope of the plot of (t/Q_t) vs. t and there is no need to know the Q_e parameter (at equilibrium) beforehand [19].

The fitting validity of these models is traditionally checked by the linear plots of $\ln(Q_e - Q_t)$ vs. t, and (t/Q_t) vs. t (figures not shown). From the slope and intersection values of the straight lines, the corresponding constant values for the pseudo-first- and pseudo-second-order kinetic models, for each temperature studied, provides the respective kinetic constants, k_i ($i = 1$ or 2), and the Q_e parameters. These kinetic parameters are shown in Tables 1 and 2.

Despite the Lagergren kinetic equations has been used for the most adsorption kinetic works, determination of possible changes

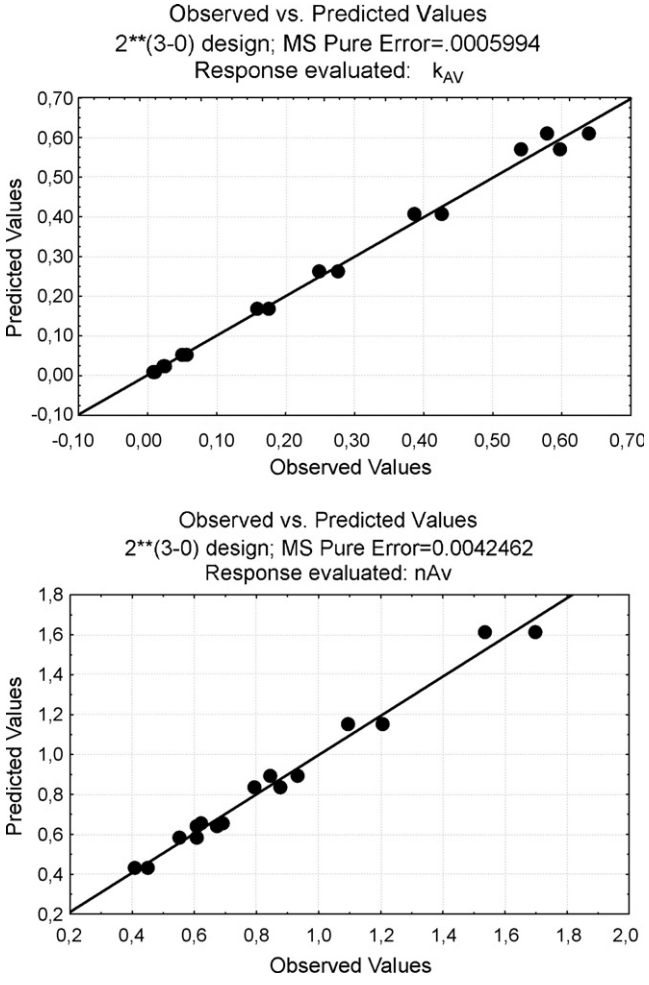

Fig. 9. Plots of observed vs. predicted values for the Avrami constants (above) and the Avrami exponents (below) in relation to the full factorial design.

Table 1
Values of the parameters of the first-order kinetic model and correlation coefficients.

Slurry	Temperature (°C)	k_1 (h^{-1})	Q_e ($\times 10^{-4}$ mol g^{-1})	r^2	χ^2
Standard	25	0.225	4.90	0.7457	1.72×10^{-9}
	35	0.060	5.42	0.9942	1.14×10^{-10}
	45	0.207	5.74	0.9686	5.62×10^{-10}
	55	0.588	5.45	0.9017	6.04×10^{-10}
GY279	25	0.010	5.35	0.9467	6.77×10^{-10}
	35	0.011	6.56	0.9863	7.91×10^{-10}
	45	0.015	6.12	0.9978	4.02×10^{-11}
	55	0.024	5.72	0.9357	5.05×10^{-10}

Table 2
Values of the parameters of the second-order kinetic model and correlation coefficients.

Slurry	Temperature (°C)	k_2 (g mol^{-1} h^{-1})	Q_e ($\times 10^{-4}$ mol g^{-1})	r^2	χ^2
Standard	25	612.81	5.30	0.9453	3.70×10^{-10}
	35	117.93	6.34	0.9788	4.22×10^{-10}
	45	385.15	6.67	0.9199	1.43×10^{-9}
	55	717.29	5.71	0.9898	6.22×10^{-11}
GY279	25	15.77	6.63	0.9513	6.18×10^{-10}
	35	13.86	8.27	0.9679	1.85×10^{-9}
	45	25.50	7.25	0.9725	5.07×10^{-10}
	55	57.64	6.38	0.9892	8.44×10^{-11}

Table 3
Values of the parameters of the Avrami kinetic model and correlation coefficients.

Slurry	Temperature (°C)	n	k_{Av} (h^{-1})	Q_e ($\times 10^{-4}$ mol g^{-1})	r^2	χ^2
Standard	25	0.43	0.167	5.43	0.9987	8.74×10^{-11}
	35	0.93	0.059	5.45	0.9954	1.04×10^{-10}
	45	1.43	0.220	5.68	0.9961	2.84×10^{-10}
	55	0.58	0.575	5.54	0.9978	1.44×10^{-11}
GY279	25	0.89	0.0094	5.52	0.9994	7.07×10^{-10}
	35	1.33	0.013	6.26	0.9980	1.31×10^{-10}
	45	1.06	0.015	6.00	0.9987	2.61×10^{-11}
	55	0.64	0.024	6.00	0.9949	4.29×10^{-11}

of the adsorption rates as a function of contact time and temperature, as well as the determination of fractionary kinetic orders represent still challenges in the kinetic studies at solid/solution interfaces. In order to overcome these limitations, the Avrami kinetic equation is also used in this work.

The adsorption should also be visualized using the Avrami exponential function shown in Eq. (8) [20]:

$$Q_t = Q_e(1 - \exp^{-[k_{Av}t]^n}) \tag{8}$$

where k_{Av} is the Avrami kinetic rate constant (min^{-1}) and n is the Avrami exponent (dimensionless), which is related to the interaction mechanism changes. The linearized form of this equation is presented in Eq. (9):

$$\ln\left(\ln\left(\frac{Q_e}{Q_e - Q_t}\right)\right) = n \ln k_{Av} + n \ln t \tag{9}$$

The slopes and intersections values provide the n and k_{Av} values, respectively. The plots (figures not shown) suggest multilinearity, indicating that two or three steps take place. So, two or three independent values of n_i (i = 1–3) and $k_{Av(i)}$ (i = 1–3) should also be considered. The Avrami kinetic parameters are shown in Table 3. The calculated n_i and $k_{Av(i)}$ Avrami constants are different from 25 to 55 °C. In this manner, the adsorption kinetic parameters seem to present both temperature and contact time dependence.

In general, it also can be found that the values of the Avrami parameters are found to increase with the rise of temperature. The GY279 slurry presents higher values for $k_{Av(i)}$ (i = 1–3) in relation the standard slurry. However, the values of n_i (i = 1–3) obtained showed no obvious increasing or decreasing trend with an increase in relation to the interaction temperature.

In order to select the best kinetic isotherm model, chi-square tests were done according to Eq. (10):

$$\chi^2 = \Sigma \frac{(Q_t - Q_m)^2}{Q_m} \tag{10}$$

where Q_t and Q_m are the HCl interaction capacities (mol g^{-1}) calculated using experimental data and an specific kinetic model, respectively. The chi-square statistic test is basically the sum of the squares of the differences between the experimental data and theoretically predicted data from models. If modeled data are similar to the experimental data, χ^2 will be a small number; if they are different, χ^2 will be a large number [21]. The analysis of the χ^2 values suggests that the interaction of the acidic species in solution can be best described by the second-order and the Avrami kinetic models, since errors between experimental and calculated values were lower for these models.

3.4. Evaluation of HCl interaction by multivariate analysis

A full 2^3 factorial design was performed to evaluate the importance of the type of slurry, concentration of HCl and temperature on the HCl interaction onto the standard and GY279 slurries. The responses evaluated were the first-step Avrami kinetic constant ($k_{Av,1}$) and the first-step Avrami dimensionless parameter (n_1), as shown in Table 4. These parameters were chosen to be evaluated in the multivariate study because they are key points to describe kinetic interactions at the solid/solution interface [18,19].

Table 4
Factors and levels used in the 2^3 factorial design study.

Factors	Levels	
	(−)	(+)
S = type of slurry	Standard	GY279
C = concentration of HCl (mol L^{-1})	0.01	0.1
T = temperature (°C)	25	55

Principal and interaction effect values are easily calculated from factorial design results. Both types of effects are calculated using Eq. (11) [22]:

$$effect = \bar{R}_{+,i} - \bar{R}_{-,i} \quad (11)$$

where $\bar{R}_{+,i}$ and $\bar{R}_{-,i}$ are average values of $k_{Av,1}$ or n_1 for the high (+) and low (−) levels of each factor. For principal or main effects the above averages simply refer to the results at the high (+) and low (−) levels of the factor whose effect is being calculated independent of the levels of the other factors. For binary interactions $\bar{R}_+$ is the average of results for both factors at their high and low levels whereas $\bar{R}_-$ is the average of the results for which one of the factors involved is at the high level and the other is at the low level. In general, high-order interactions are calculated using the above equation by applying signs obtained by multiplying those for the factors involved, (+) for high and (−) for low levels. If duplicate runs are performed for each individual measurement, as done in this work, standard errors (E) in the effect values can be calculated by [22]:

$$E = \sqrt{\frac{\sum (d_i)^2}{8N}} \quad (12)$$

where d_i is the difference between each duplicate value and N is the number of distinct experiments performed.

The results obtained in a factorial design depend, in part, on the ranges of the factors studied. The chosen levels should be large enough to cause response changes that are larger than experimental error. However, these differences should not be so large that quadratic or higher order effects due to the individual factors become important and invalidate the factorial model. Under these conditions factorial designs are particularly efficient for evaluating the principal effects of each factor and their interactions on adsorptions at the solid/solution interfaces, as well as those for academic and industrial processes [22,23].

The principal and interaction effects are presented in Table 5 and the factorial design results are in Table 6. The effect errors have presented values of $k_{Av,1} = 1.22 \times 10^{-3}$ min^{-1} and $n_{Av,1} = 0.033$. However, if the interaction terms are left out of the effect calculations (data not shown) all effect errors increase significantly.

It is observed that the results of the adsorption multivariate study have shown different behaviors in relation to the kind of "kinetic response". On average, the factors "type of slurry" and "HCl concentration" decreased the principal effects of $k_{Av,1}$ and $n_{Av,1}$. These observations are due to the diffusion extension of the acidic species into the internal parts of the slurries structures. This can be caused by the interactions of the acidic H^+ or H_3O^+ species, present in the HCl solution, with the oxygenated and nitrogenated basic sites of the chemical structures of the epoxy resins. The diffusion of the acidic species into the slurries is slower for the slurry GY279 in relation to the standard slurry [10].

Table 5
Effect values and their standard errors of the factorial design.

Effects	$k_{Av,1}$ ($\times 10^{-2}$ h^{-1})	$n_{Av,1}$
Average	0.263 ± 0.006	0.850 ± 0.016
Principal		
Q	−0.350 ± 0.012	−0.0308 ± 0.0326
C	−0.140 ± 0.012	−0.429 ± 0.0326
T	0.207 ± 0.012	0.0464 ± 0.0326
Interactions		
Q–C	0.00088 ± 0.012	0.291 ± 0.0326
Q–T	−0.0952 ± 0.012	−0.418 ± 0.0326
C–T	0.00145 ± 0.012	−0.0965 ± 0.0326
Q–C–T	−0.0983 ± 0.012	0.219 ± 0.0326

Table 6
Experimental (E) and predicted (P) results of the 2^3 factorial design.

Experiment	S	C	T	$k_{Av,1}$ (h^{-1}) E/P[a]	$n_{Av,1}$ E/P[a]
1	−1	−1	−1	0.40/0.36	0.83/0.84
2	1	−1	−1	0.05/0.09	1.61/1.20
3	−1	1	−1	0.16/0.20	0.43/0.43
4	1	1	−1	0.009/0.008	0.58/0.85
5	−1	−1	1	0.61/0.65	1.15/1.60
6	1	−1	1	0.26/0.21	0.65/0.66
7	−1	1	1	0.57/0.52	0.89/0.60
8	1	1	1	0.024/0.073	0.64/0.64

[a] Results predicted from Eqs. (13) and (14) for $k_{Av,1}$ and $n_{Av,1}$, respectively.

The $k_{Av,1}$ parameter increases with increasing temperature. However, the binary effect "Slurry–Temperature" and the ternary effect "Slurry–Concentration–Temperature" were very important in the analysis of this important kinetic parameter. A similar behavior is also observed in relation to the importance of the interaction effects of the $n_{Av,1}$ parameter. In this case, almost all principal effects are only marginally important in relation to the effect errors shown in Table 3.

3.4.1. Adsorption polynomial modelings

Quantitative polynomial models for $k_{Av,1}$ and $n_{Av,1}$ can be written in terms of the statistically significant effects in Table 5 [22]:

$$k_{Av,1}\,(\times 10^{-2}\,h^{-1}) = 0.265 - 0.175x_1 - 0.0701x_2 + 0.103x_3 - 0.0476x_1x_3 - 0.0492x_1x_2x_3 \quad (13)$$

$$n_{Av,1} = 0.850 - 0.215x_2 + 0.146x_1x_2 - 0.209x_1x_3 - 0.048x_2x_3 + 0.109x_1x_2x_3 \quad (14)$$

where x_1, x_2 and x_3 are codified (±1) values of slurry, concentration of HCl and temperature, respectively.

The experimental and predicted values of $k_{Av,1}$ and $n_{Av,1}$ are also shown in Table 6, as well as in Fig. 9. In general, good correlations were observed for the observed and predicted values of and $k_{Av,1}$ and $n_{Av,1}$.

4. Conclusions

In this study, an epoxy-modified cement slurry was synthesized. The characterization techniques used have indicated significant compositional differences in relation to the standard slurry. The XRD patterns, as well as the TG/DTG and DSC analyses have confirmed the absence of portlandite in the epoxy-modified cement slurry. The characterization of the slurries after HCl attack suggests possible recrystallization of some slurries constituents.

The kinetic data of the interaction of the acidic species of HCl solution with the epoxy-modified cement slurry were best fitted to the second-order and the Avrami kinetic models.

It is noted that the interaction of HCl onto cement slurries, from the factorial design point of view, is a complex phenomenon. The type of slurry and HCl concentration present more significance in the Avrami kinetic constants $k_{Av,1}$. However, the best modelings for the kinetic parameters were obtained using some binary and ternary interactive effects.

Evidently, additional standard testing procedures must also be performed in order to use the epoxy-modified cement slurry in long-term oilwell cementing operations. However, the characterization and the factorial design results have suggested that the epoxy-modified slurry presents a good potential, from the chemical and morphological viewpoints, to be used as an alternative reinforcing material in environmental-friendly oilwell operations.

References

[1] P.C. Hewlett (Ed.), Lea's Chemistry of Cement and Concrete, Elsevier, Burlington, 1998.
[2] G. Le Saout, E. Lecolier, A. Rivereau, H. Zanni, Chemical structure of cement aged at normal and elevated temperatures and pressures. Part II. Low permeability class G oilwell cement, Cement Concrete Res. 36 (2006) 428–433.
[3] G. Le Saout, E. Lecolier, A. Rivereau, H. Zanni, Study of oilwell cements by solid-state NMR, C. R. Chim. 7 (2004) 383–388.
[4] D.A. Silva, P.J.M. Monteiro, Hydration evolution of C3S–EVA composites analyzed by soft X-ray microscopy, Cement Concrete Res. 35 (2005) 351–357.
[5] H. Hodne, A. Saasen, A.B. O'Hagen, S.O. Wick, Effects of time and shear energy on the rheological behaviour of oilwell cement slurries, Cement Concrete Res. 30 (2000) 1759–1766.
[6] J.J. Chen, D. Zampini, A. Walliser, High-pressure epoxy-impregnated cementitious materials for microstructure characterization, Cement Concrete Res. 32 (2002) 1–7.
[7] R.E. Beddoe, H.W. Dorner, Modelling acid attack on concrete. Part I. The essential mechanisms, Cement Concrete Res. 35 (2005) 2333–2339.
[8] H.W. Dorner, R.E. Beddoe, Prognosis of concrete corrosion due to acid attack, in: Proceedings of the 9th International Conference of Building Materials, Brisbane, Australia, 2002.
[9] K. Svinning, A. Høskuldsson, H. Justnes, Prediction of compressive strength up to 28 days from microstructure of Portland cement, Cement Concrete Compos. 30 (2008) 138–151.
[10] A.R. Cestari, E.F.S. Vieira, A.A. Pinto, F.C. da Rocha, Synthesis and characterization of epoxy-modified cement slurries—kinetic data at hardened slurries/HCl interfaces, J. Colloid Interf. Sci. 327 (2008) 267–274.
[11] E.F.S. Vieira, A.R. Cestari, R.G. da Silva, A.A. Pinto, C.R. Miranda, A.C.F. Conceição, Use of calorimetry to evaluate cement slurry resistance to the attack of acid solutions, Thermochim. Acta 419 (2004) 45–49.
[12] A.R. Cestari, E.F.S. Vieira, F.C. da Rocha, Kinetics of interaction of hardened oilwell cement slurries with acidic solutions from isothermal heat-conduction calorimetry, Thermochim. Acta 430 (2005) 211–215.
[13] A. Hidalgo, S. Petit, C. Domingo, C. Alonso, C. Andrade, Microstructural characterization of leaching effects in cement pastes due to neutralisation of their alkaline nature. Part I. Portland cement pastes, Cement Concrete Res. 37 (2007) 63–70.
[14] F. Djouani, C. Connan, M.M. Chehimi, K. Benzarti, Interfacial chemistry of epoxy adhesives on hydrated cement paste, Surf. Interf. Anal. 40 (2008) 146–150.
[15] V.L. Zvetkov, R.K. Krastev, V.I. Samichkov, Rate equations in the study of the DSC kinetics of epoxy-amine reactions in an excess of epoxy, Thermochim. Acta 478 (2008) 17–27.
[16] R. Mezzenga, L. Boogh, J.-A.E. Månson, A review of dendritic hyperbranched polymer as modifiers in epoxy composites, Compos. Sci. Technol. 61 (2001) 787–795.
[17] B. Lothenbach, G. Le Saout, E. Gallucci, K. Scrivener, Influence of limestone on the hydration of Portland cements, Cement Concrete Res. 38 (2008) 848–860.
[18] Y.S. Ho, Selection of optimum sorption isotherm, Carbon 42 (2004) 2113–2130.
[19] Y.S. Ho, G. McKay, Sorption of dyes and copper ions onto biosorbents, Process Biochem. 38 (2003) 1047–1061.
[20] E.C.N. Lopes, F.S.C. dos Anjos, E.F.S. Vieira, A.R. Cestari, An alternative Avrami equation to evaluate kinetic parameters of the interaction of Hg(II) with thin chitosan membranes, J. Colloid Interf. Sci. 263 (2003) 542–547.
[21] M.C. Ncibi, Applicability of some statistical tools to predict optimum adsorption isotherm after linear and non-linear regression analysis, J. Hazard. Mater. 153 (2008) 207–212.
[22] R.E. Bruns, I.S. Scarminio, B.B. de Barros Neto, Statistical Design—Chemometrics, Elsevier, Amsterdam, 2006.
[23] A.R. Cestari, E.F.S. Vieira, J.A. Mota, The removal of an anionic red dye from aqueous solutions using chitosan beads—the role of experimental factors on adsorption using a full factorial design, J. Hazard. Mater. 160 (2008) 337–343.